ROTATIONAL SPLITTINGS WITH COROT, EXPECTED NUMBER OF DETECTION AND MEASUREMENT ACCURACY

M.J. Goupil [1], J. Lochard[1], R. Samadi[1], C. Barban[1], M.A. Dupret[1], and A. Baglin[1]

[1] *Laboratoire d'Etudes Spatiales et d'Instrumentation pour l'Astrophysique, UMR CNRS 8109, Observatoire de Paris, 5 place J. Janssen, 92190, Meudon, France*

ABSTRACT

One of the main goal of the CoRoT experiment is to determine the internal rotation of stars. A seismic measure of rotation requires the detection and an accurate measurement of rotational splittings. Our ability to achieve this goal with CoRoT observations depends on the properties of the target star (in short: spectral type and distance) and will be discussed.

1. INTRODUCTION

Seismology can be a power tool to provide information about stellar rotation through the precise knowledge of the frequency splittings. The question is however whether these splittings will be detected with CoRoT; if they are, how many of them; which precision will have the measurements and what information will they provide, for whar star?. These issues are adressed in this work which has been presented at the second CoRoT Brasil meeting (2005).

The oscillation eigenmodes of a stellar non rotating model can be represented with a single spherical harmonics $Y_{\ell,m}$; the associated eigenfrequencies $\nu_{n\ell}$ are $2\ell+1$ *degenerate* as they do not depend on the azymuthal number m; n is the radial order of the mode.

Stellar rotation breaks the spherical symmetry of a star and thereby lifts the degeneracy : a mode with given n, ℓ gives rise to a multiplet of $2\ell+1$ components with associated eigenfrequencies $\nu_{n,\ell,m}$.

If the rotation rate, Ω, is not too large ($\Omega^2/(GM/R^3) < 0.01-0.1$ with M and R the mass and radius of the star, G the gravitational constant), the rotation can be treated as a perturbation. The first order correction to the eigenfrequency comes from the Coriolis force; it can be written under the form $\Delta\nu_{n,\ell,m} = \nu_{n,\ell,m} - \nu_{n,\ell} = m\ \Delta\nu_{n\ell}$ and is a measurable quantity.

The rotational splittings, $\Delta\nu_{n\ell}$, are related to the rotation rate (or rotational angular velocity in rad/s) inside the star as:

$$\Delta\nu_{n\ell} = \int \frac{\Omega(r,\theta)}{2\pi}\ K_{n,\ell}(r,\theta) d\theta dr$$

where r is the radius inside the star, $K_{n,\ell}$ is the rotational kernel which depends on the eigenfunction associated with the (n,ℓ) nonrotating mode. From the knowledge of the splittings (determined observationally), it is then theoretically possible to invert the above relation and deduce the rotation profile $\Omega(r,\theta)$.

We consider here only the depth dependence of the rotation profile and therefore look for information on $\Omega(r)$ which satisfies (see for intance, Christensen-Dalsgaard, 2003):

$$\Delta\nu_{n\ell} = \int_0^R \frac{\Omega(r)}{2\pi}\ K_{n,\ell}(r) dr \qquad (1)$$

where

$$K_{n,\ell} = \frac{1}{I}(\xi_r^2 + \Lambda\xi_t^2 - 2\xi_r\xi_t - \xi_t^2)\rho r^2 dr\ \ ;\ \Lambda = \ell(\ell+1) \qquad (2)$$

and

$$I = \int_0^R\ (\xi_r^2 + \Lambda\xi_t^2)\rho r^2 dr \qquad (3)$$

where ρ is the stellar density, ξ_r and ξ_t and are the radial and horizontal displacement eigenfunctions (Unno et al., ..).

If rotation is uniform inside the star, the splittings reduce to

$$\Delta\nu_{n,\ell} = \nu_{rotsurf}\ (1 - C_{n,\ell}) \qquad (4)$$

in the observed frame with the Ledoux constant given by:

$$C_{n\ell} = \frac{1}{I}\int_0^R\ (2\xi_r\xi_t + \xi_t^2)\ \rho r^2 dr$$

and $\nu_{rotsurf} = \Omega_s/(2\pi)$ with Ω_s the surface rotation rate.

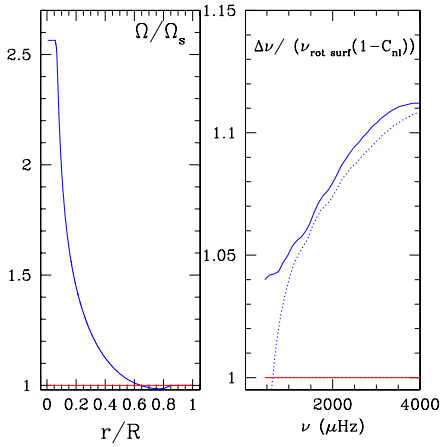

Figure 1. Top: Schematic rotation profile as it would be obtained assuming local conservation of angular momentum (blue) and uniform rotation (red) both normalized to the surface rotation rate Ω_s. Bottom: $\Delta\nu_{n,\ell}/(\nu_{rotsurf}(1-C_{n\ell}))$ for $\ell = 1$ modes in function of the corresponding frequency $\nu_{n,\ell}$. The rotational splittings $\Delta\nu_{n,\ell}$ are computed using Eq.5 with the rotational profile displayed on the left for $\ell = 1, 2$ modes (solid and dotted blue curves resp.) and computed assuming uniform rotation (Eq.4) (red curves).

For nonuniform rotation, we consider

$$\Delta\nu_{n,\ell} = \nu_{rotsurf} \int_0^R \frac{\Omega(r)}{\Omega_s} K_{n,\ell}(r)dr \qquad (5)$$

For a uniform rotation and a given star, the splittings are the same apart from the Ledoux constant $C_{n\ell}$ (Eq.1). On the other hand, the signature of a varying rotation rate, $\Omega(r)$, with depth on the splittings is a variation of the splitting value with the mode frequency since different modes probe different depths. Fig.1 illustrates this behavior for a 1.25 $M_\odot$ stellar model with a stellar radius of 1.31 $R_\odot$ and effective temperature $T_{eff} = 6420K$. The horizontal curve represents the case of uniform rotation $\Omega(r) = \Omega_{surf}$. The varying curves correspond to splittings which vary with the modes because the assumed rotation profile varies with depth as shown on Fig.1(left).

It is this property which enables to probe the internal rotation profile of an oscillating star.

When adressing the aforementionned issues, one must first distinguish two different cases:

• *Opacity driven oscillations* concern δ Scuti, β Cephei, γ Dor stars which are intermediate mass (1.5 to $\sim$ 7 $M_\odot$) stars on the main sequence. For such stars, modes are self excited by the κ mechanism which generates oscillations with large amplitudes.

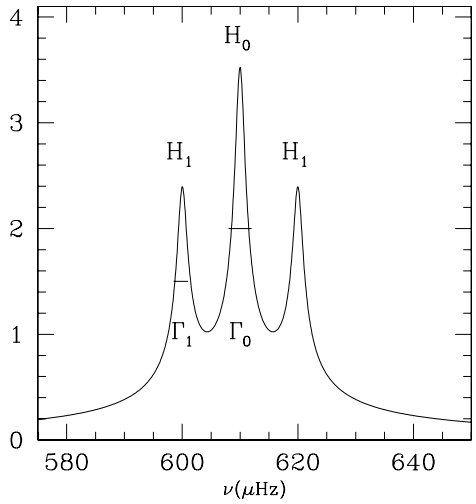

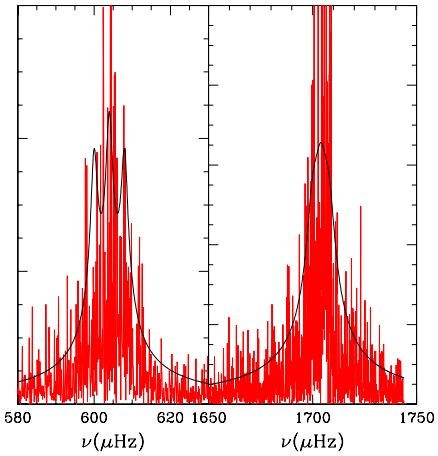

Figure 2. Top: a schematic representation of a $\ell = 1$ multiplet split by (a slow) rotation when the oscillations have a finite life time. H_1, H_0 are the heigths of the $m = 0$ and $m = \pm 1$ modes while Γ_0, Γ_1 are the widths of these modes respectively. Bottom: simulation of two damped, stochastically excited $\ell = 1$ multiplets split by rotation in a power spectrum: the left one is a resolved triplet whereas the right one is not resolved ($bin = 0.1\mu Hz$) for a 1.4 $M_\odot$ TAMS model with $i = 60°$ and $\Delta\nu = 4\mu Hz$, left: $\Gamma = 1.8\mu Hz$ for typical $\nu_0 = 600\mu Hz$; right , $\Gamma = 6.\mu Hz$ for typical $\nu_0 = 1700\mu Hz$. The solid curves represent average profiles, the fluctuations simulating the result of the stochastic excitation have been built with a random number generator.

These oscillations are coherent hence their width is given by the observing time $\sim 1/T_{obs}$.

These stars are rather fast rotators and there should be any problem in detecting their splittings. The problem with these stars lies elsewhere : it will not be easy to say which mode is associated with which detected frequency, the so-called mode identification problem. As this is out of scope here, these stars will not be discussed any further (see for instance Goupil et al 2004, Suarez et al 2006, Reese et al 2006).

• *Stochastically excited, damped oscillations*: also named solar like oscillations. These p-modes are excited by turbulent convection in the upper convective regions of the star. This concerns main sequence stars with relatively low mass to have an enough extended outer convective region. For a long time, the Sun was the only star which showed this type of oscillation. These oscillations are damped, that-is the kappa mechanism is not operating efficiently to cause these modes to be unstable. Left to themselves, these modes would rapidly die (over $\sim$ 5 days). However turbulent convection in the outer layer transfers acoustic energy into these oscillations which then are stochastically excited. Amplitudes of such oscillations are much smaller (a few ppm) than in the previous case and only recently they have been firmly detected in other stars. We know now several solar like oscillating stars: Procyon (Martic et al. 1999, Barban et al. 1999), α Cen (Bouchy et al .), HD49933 (Mosser et al 2005), η Boo (see references section). These stars are rather low mass, slow rotator stars. If the rotation is too slow, their rotational splittings can happen to be smaller than the width of the modes, Γ, and therefore would not be detectable. Hence some constraints on the ratio of the width over the splitting must be considered in order to expect detection of splittings.

Because these modes are stochastically excited by turbulent convection and have a finite life time ($\tau = 2\pi/\Gamma$)), their average profile in a power spectrum is lorentzian and is given by (Fig.2(left)):

$$P(\nu) = \frac{H\ (\Gamma/2)^2}{(\nu - \nu_0)^2 + (\Gamma/2)^2} + noise \qquad (6)$$

where the height H is related to the intrinsic amplitude of the mode A (see Baudin et al, this volume; Baudin et al., 2005) Fig.2(right) shows two illustrative cases: two $\ell = 1$ modes which are split by rotation, hence two triplets of modes with $m = -1, 0, 1$ (from spherical harmonics). We assume the same expression Eq.4 for all the multiplet components with A given by the amplitude of the $m = 0$ modified by visibility effect. Here we take a inclination angle $i = 30°$. We consider one solar like oscillation mode of low frequency which is rather narrow and a second mode with higher frequency which therefore is wider. In the first case, the splitting is larger than the width of each component, the triplet can be resolved and the splitting detected. This is no longer true in the second case.

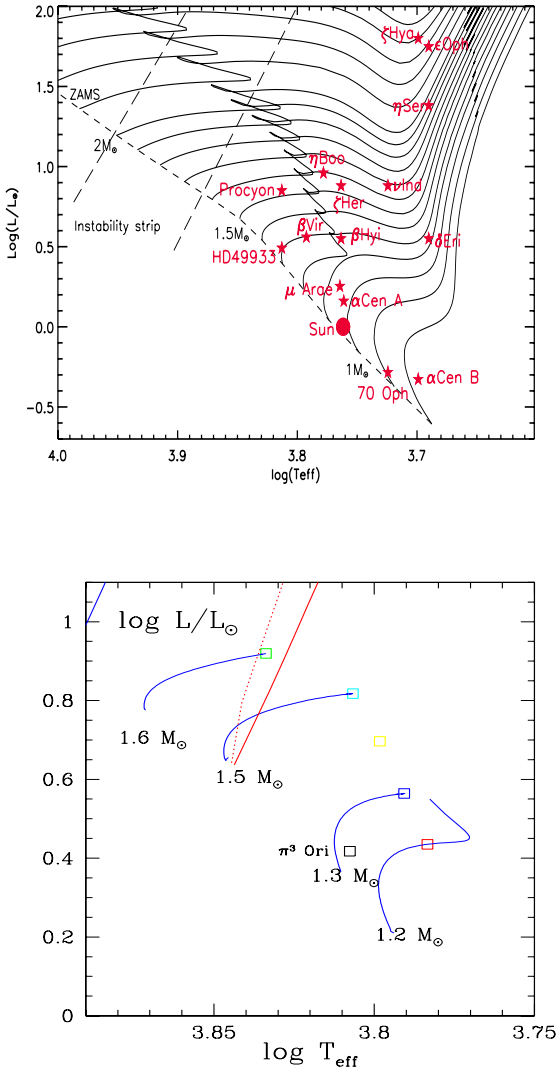

Figure 3. Top: HR diagram which shows the location of stars which have been observed to undergo solar like oscillations; Bottom HR diagram showing selected models (squares) and their evolutionary tracks from the ZAMS. Also indicated a selected model which represents a target star of CoRoT π^3 Ori. The red curves delimitate the classical instability strip for opacity driven pulsators for $\ell = 0, 2$ modes (solid, dashed curves resp.). In the very upper part of the left corner, the blue side of the instability strip for radial modes is visible.

2. WHAT CAN WE EXPECT AS DETECTION AND MEASUREMENT ACCURACY OF ROTATIONAL SPLITTING?

The second step, once the splittings have been detected, is to measure them accurately enough to obtain useful information about stellar rotation and this requires a high signal to noise ratio as seen next.

In order to estimate the number of detected splittings as well as their measurement accuracy in function of the considered star, we use simple simulations as detailed below. Note that Gizon & Solanki (2003,2004) have carried out Montecarlo simulations and reach similar conclusions.

2.1. Detection criteria

As mentionned above, the first step is to establish a detection criterion.

Criterion 1: Here we assume that a $m \neq 0$ component can be detected if its signal to noise ratio, SNR, satisfies :

$$SNR > 9 \tag{7}$$

as measured in the power spectrum (hence a SNR detection level of 3 in amplitude).

Criterion 2: The splittings must be large enough compared to the widths of the adjacent components of a multiplet. For a $\ell = 1$ multiplet for instance, one imposes: $\Delta\nu > (\Gamma_0 + \Gamma_1)/2 \sim \Gamma_0$ where Γ_0, Γ_1 are the widths of the $m = 0, m = \pm 1$ respectively. More generally, we assume as an additional detection criterion that a splitting is detected if it is larger than the width of the $m = 0$ mode:

$$\Delta\nu > \Gamma \tag{8}$$

2.2. Expected signal to noise ratio and measurement uncertainties

In criterion 1, Eq.7, the signal to noise ratio $SNR = SNR(A_1, m_v)$ depends on the amplitudes of the $m \neq 0$ components, A_1, and on the noise level which itself in practice depends on the apparent magnitude of the star m_v.

The amplitudes of the $m \neq 0$ components A_1 can be related to the $m = 0$ one, A_0: the ratio A_1/A_0 is assumed to depend only on visibility effects (although not necessarily true) which depend on the inclination angle i. Amplitudes A_0 and widths Γ_0 of the excited modes are in turn dependent on the mass and age of the star.

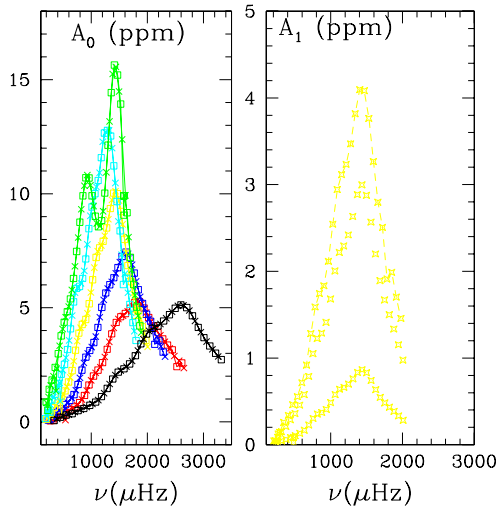

Figure 4. Top: Amplitudes in intensity, A_0, for $m = 0$ modes in function of frequency for the selected models of Fig.3: red:1.2 $M_\odot$ TAMS; dark blue: 1.3 $M_\odot$; yellow: 1.4 $M_\odot$ TAMS; light blue: 1.5 $M_\odot$; green: 1.6 $M_\odot$ TAMS; black: 1.3 $M_\odot$ ZAMS (π^3 Ori); bottom: Amplitudes A_1 of $m \neq 0$ components of $\ell = 1, 2$ modes for the $1.4 M_\odot$ TAMS model with $i = 60°$.

The signal to ratio also depends whether the mode is resolved or not (see Lochard et al., 2005). This is also true for the splitting measurement precision as detailed next.

2.2.1. Resolved modes

A *resolved* mode has its width, Γ, which is larger than the frequency bin, $bin = 1/T_{obs}$ with $T_{obs} =$ the observation time interval.

CoRoT specifications estimate the noise level B^2 in a power spectrum for a target star with an apparent magnitude $m_0 = 5.7$ mag at $(0.61)^2$ ppm^2 for a width $\Gamma_{n\ell} = 1 \mu Hz$. More generally, we expect for a star with an apparent magnitude m_v and a mode line width $\Gamma_{n\ell}$.

$$B^2 = \frac{(0.61)^2}{2.3}\, 10^{\frac{m_v - m_0}{2.5}} \quad ppm^2$$

(Note that this takes into account the white noise level for CoRoT but does not include other perturbations such as stellar activity for instance but also orbital noises and long term instrument response)

Hence the signal to noise for a star with apparent magnitude m_v, and a given $(n\ell)$ mode, with a width

$\Gamma_{n\ell}$ and an oscillation amplitude A_1 is obtained as:

$$SNR = \left(\frac{A_1}{0.61}\right)^2 \frac{2.3}{\pi\Gamma_{n\ell}} 10^{-\frac{(m_v-m_0)}{2.5}} \quad (9)$$

Splitting uncertainty When the splitting is detected (ie satisfying Eq.7 and Eq.8), the precision of its measurements (σ in μHz) is calculated according (Libbrecht, 1992):

$$\sigma^2 = \frac{\Gamma_{n\ell}}{4\pi T_{obs}} \sqrt{\beta+1}\left(\sqrt{\beta+1}+\sqrt{\beta}\right)^3 \quad (10)$$

with $\beta = 1/SNR$

The SNR drops rapidely with the apparent magnitude of the star and for a given star with its distance. For instance, a 100pc star has $SNR = 0.01 SNR_{(10pc)}$ and for a 500pc star, $SNR = 4\ 10^{-4} SNR_{(10pc)}$. This considerably reduces the number of detected splittings and increases their measurement uncertainties. This is illustrated in Fig.6 below.

2.2.2. Nonresolved modes

A *nonresolved* mode has a width which is smaller than 1 bin ie longlife time mode: $\Gamma_{n,\ell} < bin = 1/T_{obs}$, then SNR varies with the magnitude m_v as:

$$SNR = 0.5\ (\frac{A1}{0.61})^2 \frac{T_{obs}(\text{in days})}{5}\ 10^{\frac{-(m_v-m_0)}{2.5}} \quad (11)$$

Splitting uncertainty When the splitting is detected (ie satisfying Eq.7 and Eq.8), the precision of its measurement is given by

$$\sigma = 1/T_{obs} = 0.08 \mu Hz \quad (12)$$

for $T_{obs} = 150$ days.

2.3. Simulations

For a given stellar model, i.e. given $T_{eff}, L/L_\odot$, we compute the number of detected splittings, N_s ie which satisfy the detection criteria Eq.7 and Eq.8.

As input we need the apparent magnitude hence the luminosity (hence the mass) and the distance; we need the splitting values (hence $\nu_{rotsurf}$, hence the rotational velocity and the stellar radius), the inclination angle i and the observing time interval T_{obs}.

We consider TAMS models with masses ranging from 1.2 to 1.6 $M_\odot$ and one younger MS 1.25 $M_\odot$ star representative of π^3 Ori. The selected models are computed with CESAM code (Morel, 1997) and their evolutionary tracks in a HR diagram are shown in Fig.3.

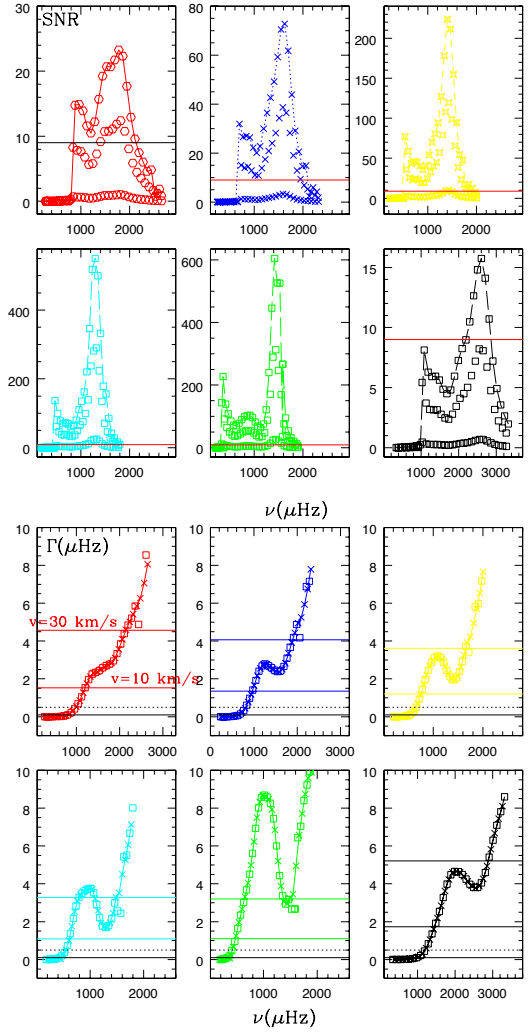

Figure 5. Top: Signal to noise ratio, SNR, Inclination angle has been set to 30°. Colours have the same meaning as in Fig.4. The horizontal line represents the detection threshold $SNR = 9$. Modes above this threshold are considered as detectable. (A 10 pc distance and $T_{obs} = 150$ days have been assumed). Bottom: Width of each mode plotted in function of its frequency. The coloured horizontal lines represent the splitting values for for the corresponding rotation rate. The horizontal black lines represent the frequency bin values for $T_{obs} = 150$ days (solid) and 20 days (dashed). Modes above these line are resolved.

To proceed, we obtain the necessary input ingredients, m_v, $\nu_{n\ell}$, $\Gamma_{n\ell}$, $\Delta\nu_{n\ell}$, SNR as follows:

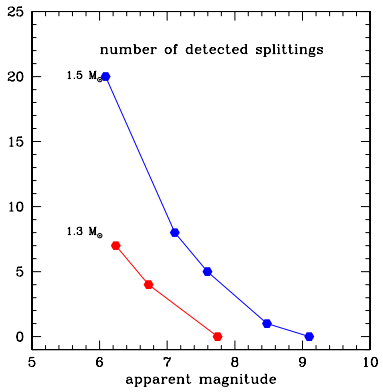

Figure 6. Number of detected splittings as a function of the apparent magnitude for a 1.5 $M_\odot$ TAMS star and a 1.3 $M_\odot$ TAMS star (T_{obs} = 150 days, $i = 80°, v = 30$ km/s).

• The luminosity is converted in absolute magnitude with $M_{bol} = 4.64 - 2.5 \log_{10}(L/L_\odot)$, then assuming the star is at a distance d (in pc), one derives the apparent magnitude (neglect the bolometric correction) as $m_v = M_{bol} + 5 \log_{10} d - 5$.

• Adiabatic frequencies $\nu_{n,\ell}$ with $\ell = 1, 2$ are computed in the frequency interval [$\sim$ 100,$\sim$ 3200] μ Hz with the adiabatic oscillation code ADIPLS (Christensen-Dalsgaard et al., 1996)

• we take the corresponding damping rates $\Gamma_{n,\ell}$ (displayed in Fig.5) from Houdek's Tables (Houdek et al., 1999)

• We compute the excitation rates as in Samadi, Goupil (2001) and Samadi et al. (2003), details can be found in Baudin et al., this volume. The excitation rates are combined with the damping rates $\Gamma_{n\ell}$ to provide the intensity amplitudes of $m = 0$ modes, A_0 . These are shown in Fig.4. We compute the amplitudes of $m \neq 0$ components, A_1 as $A_1 = A_0\ Q_{\ell,m}(i)$ where $Q_{\ell,m}(i)$ are the visibility coefficients for ℓ, m modes for various inclination angle i. We consider four values for $i = 10°, 30°, 60°, 80°$ (see Table 1). As we have neglected the effect of limb darkening in the visibility coefficients, these vanish for $\ell = 3$ and we limit the study to splittings of $\ell = 1, 2$ modes.

The signal to ratio, $SNR(A_1)$ are then computed using Eq.9 and Eq.11.

• The splittings $\Delta\nu_{n,\ell}$ are given by Eq.4 as we assume a uniform rotation for sake of simplicity (see section 4.2 for a discussion about a nonuniform rotation) . We consider several values of the rotational velocity

	i=10°	i=30°	i=60°	i=80°
Q_{10}	1.137	1.000	0.577	0.201
$Q_{1\pm1}$	0.142	0.408	0.707	0.804
Q_{20}	0.534	0.349	0.070	0.254
$Q_{2\pm1}$	0.117	0.296	0.296	0.117
$Q_{2\pm2}$	0.010	.0856	0.257	0.332

Table 1. Visibility coefficients, $Q_{\ell m}$, in intensity, I, for different values of inclination angles, i.

$v = 10, 30, 50$ km/s and compute $\nu_{rotsurf} = v/(2\pi R)$ with the radius of the stellar model.

Their measurement accuracy, σ, is computed according to Eq.10 and Eq.12. As σ depends on T_{obs}, the observing time interval, we assume T_{obs} = 150 days (long run).

Criteria 1 (Eq.9) and 2 (Eq.11) are then applied. The results are summarised in Fig.5 which shows that the number of splittings with $SNR > 9$, N_s increases with the mass and age of the star. We also see that the modes rapidely become too wide with increasing frequency to be detectable according to criterion 2. Furthermore, as it can be expected, for a given star, N_s increases with the rotational velocity v as the splittings then get larger and criterion 2 easier to be satisfied. We note also that except at very low frequency, most modes are resolved.

2.4. Influence of inclination angle, mass, age, surface rotational velocity, distance

Fig.7 represents the number of detected splittings as well as their measurement uncertainties in function of their $m = 0$ frequency for several values of the surface velocity and inclination angle. This representation is given for a 1.3 ZAMS model, a 1.3 TAMS model and a 1.5 ZAMS model. The detected splittings are represented with different colours depending on the inclination angle. The nondetected splittings are shown in black symbols at the bottom of the panels.

We find that the number of detected splittings (i.e. satisfying both criteria), N_s, increases age , surface rotational velocity and inclination angle. This can be easily understood with the dependence of SNR and σ upon these quantities as discussed in the previous section. N_s also increases with the mass for masses up to 1.4 $M_\odot$. Above this mass, the theoretical widths of the modes become quite large and the number of detected splitting can decrease. This must be taken with caution as theoretical computation of mode line widths remains very dubious.

The measurement uncertainties also follow quite closely the behavior of the mode line widths. When

the modes are detected , their measurement precision lies in the range $\sigma \sim 0.1 - 0.3 \mu Hz$

For sake of simplicity, we have sofar investigated $1.2 M_\odot - 1.6 M_\odot$ stars located at 10 pc. We now consider more realistic cases where these stars are further away, hence with significantly higher apparent magnitudes. This causes the signal to noise ratio to decrease hence the number of detected splittings to decrease. The number of detected splittings as computed from our simulations is plotted in Fig.6 as a function of the apparent magnitude of the star. Splittings are no longer detected for a 1.5 $M_\odot$ star with apparent magnitude above 8.5 and for a 1.3 $M_\odot$ above 7.5.

3. COMPARISON WITH RESULTS FROM A HARE AND HOUND EXERCISE ABOUT HD49333

HD 49333 is a 1.25 $M_\odot$ star with en effective temperature $T_{eff} \sim 6700K$. As it was considered as a possible CoRoT target, it was chosen as a proxy star for a Hare and Hound exercise by the CoRoT HH team (see Appourchaux et al in the same volume). Since then, it was observed from ground with Harps and was shown to undergo solar like oscillation (Mosser et al, 2005). Many splittings were indeed detected. As expected, the error bars on the splitting measurements were found to increase with the frequency. Characteristics of this star corresponds approximately to the π Ori model studied here with a rotational velocity of 10 km/s in Fig.7. HH results confirm the present estimation in this case that only a few splittings can be detected with uncertainties below 0.5 μHz.

4. WHAT PIECES OF INFORMATION UPON ROTATION CAN WE EXPECT FROM THESE SEISMIC MEASUREMENTS?

We can consider 3 levels:

• *Level 1* Only a few splittings with enough precision are detected. Then a readily straightforward average of the splittings yields the surface rotation period.

• *Level 2* Enough splittings with enough precision are detected so that a forward method can provide some information on the r-profile of the rotation rate inside the star.

• *Level 3* Enough splittings with enough precision with appropriate nature are detected so that an inversion technique can provide some information upon the r-profile of the rotation rate deep inside the star. This third level will be obtained only for specific stars ie with masses above $1.4-1.5 M_\odot$ and evolved enough (middle of the main sequence) with an apparent magnitude below 7.

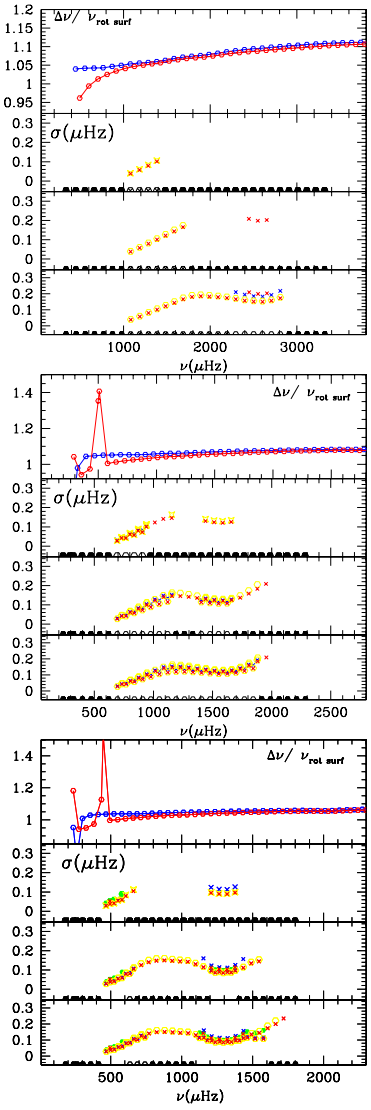

Figure 7. Top panel: π^3 Ori: a 1.25 $M_\odot$ ZAMS model. From top to bottom: splittings calculated with a non uniform rotation; uncertainties σ for detected splittings assuming a surface velocity of $v = 10$ km/s; $v = 20$ km/s; $v = 30$ km/s. middle panel same for a 1.3 $M_\odot$ TAMS model. bottom panel Same for a $1.50 M_\odot$ TAMS model. Colours corresponds to different inclination angles as in Fig.6 (distance =10pc, $T = 150$ days).

4.1. Level 1

At level 1, stars with apparent magnitude above 8 are too faint to allow the detection of enough precisely measured splittings for a forward technique to be used. However an average rotation period can be determined as the average over the detected splittings as

$$P_{rot}^{-1} = < \frac{\Delta\nu_{n,\ell}}{1 - C_{n\ell}} > = \frac{1}{N_s} \sum_{j=1,N_s} \frac{\Delta\nu_j}{1 - C_j} \qquad (13)$$

Note that the average rotation period, P_{rot}, which is determined by seismic measurements is an average of the rotation period over a depth where the modes propagate which extends downward the surface; hence it can differ from the surface rotational period P_{surf} which would be obtained with spot techniques for instance.

Our simulations show that the difference $|P_{rot} - P_{surf}|$ amounts to about a few hours where we have assumed a surface rotational period of about a few days; this is slightly larger than the measurement uncertainty on P_{rot}.

4.2. Level 2

Fig.7 shows that the splittings which are expected to be detected are not equal but vary with the frequency, which indicates that the rotation is not uniform. Let crudely represent the rotation profile in Fig.2 as:

$$\Omega(r) = \Omega_c \quad \text{for } r \leq r_c \quad ; \qquad \Omega(r) = \Omega_s \quad \text{for } r > r_c \qquad (14)$$

We then easily find from Eq.5:

$$\frac{\Delta\nu_{n\ell}}{\nu_{rotsurf}} = \Big(\frac{\Omega_c}{\Omega_s} - 1\Big) \int_0^{r_c} K_{n\ell}(r)\, dr + \Big(1 - C_{n\ell}\Big) \qquad (15)$$

As an example, let consider the splitting, $\Delta\nu_1$ of the highest frequency in the detected splitting set and $\Delta\nu_2$ the splitting of the lowest frequency one for a given ℓ. Then one obtains:

$$\Big(\frac{\Omega_c}{\Omega_s} - 1\Big) = \frac{1 - C_1 - (1 - C_2)(\Delta\nu_1/\Delta\nu_2)}{K_2(\Delta\nu_1/\Delta\nu_2) - K_1} \qquad (16)$$

where $K_j = \int_0^{r_c} K_{n_j,\ell_j} dr$ (j=1,2) with r_c the radius of the convective core. This crude modelling can tell us whether the core rotates faster than the surface.

For instance, in the case of $\ell = 1$ modes for the π^3 Ori model and a rotational surface velocity $v = 20$ or 30 km/s (Fig.10left), one has $\nu_1 = 1.08mHz; \nu_2 = 2.5mHz; \Delta\nu_1/\Delta\nu_2 = 1.06$ and $K_1 = 0.054$, $K_2 = 0.0245$, $1 - C1 = 0.994 \sim 1$, $1 - C2 = 0.983 \sim 1$. This yields $\Omega_c/\Omega_s \sim 1.95$ (to be compared with the true value 2.56). Hence with a modelling as crude as Eq.16, one can already conclude that the core rotates faster than the surface by a ratio larger than $\sim 1.95-2$

More sophisticated profiles of course can be implemented into Eq.5 and the results compared to the observed splittings for further constraints upon rotation.

As the mass and age of the model increase, the lowest frequency detected splittings reach those which are associated with mixed modes (large values of the splittings) which makes possible a successful inversion process as illustrated next.

4.3. Level 3

The inversion of the splittings requires a larger variety of modes than the previous levels. It is known that one cannot retrieve localized information about the internal rotation profile with only low degree ($l \leq 3$) pure p modes. However for a star with appropriate mass and age, it is expected to detect enough splittings to perform an inversion of the data and obtain the rotation rate in the deep parts of the star. Indeed, stars with a convective core and evolved enough can present modes that probe the deep inside of the star, down to the edge of the core. Such modes, called *mixed modes*, have dual characteristics as they share their energy both in the inner and outer layers of the star. Lochard et al. (2005) showed that the detection of only a few mixed modes would be enough to perform an inversion of the splittings and recover localized information on the rotation rate at several radii close to the core, leading to an estimate of the expected gradient. Figure 8 shows the reconstructed profiles from the values obtained at these radii.

This study gave constraints to select such appropriate stars from their mass, evolution stage and surface rotation rate. Among the stars CoRoT will observe, 5 answer the selection criterions. Their characteristics are presented in Tab. 2.

HD	$M/M_\odot$	m_v	$V\ sini$ (km/s)
170987	1.4	7.5	20.6
170579	1.3	7.5	13.5
171802	1.5	5.39	14
181420	1.3	6.57	21.1
171834	1.5	5.45	72.1

Table 2. List of potential targets in the CoRoT fields that would suit for radial rotational profile inversion. All stars are F spectral type.

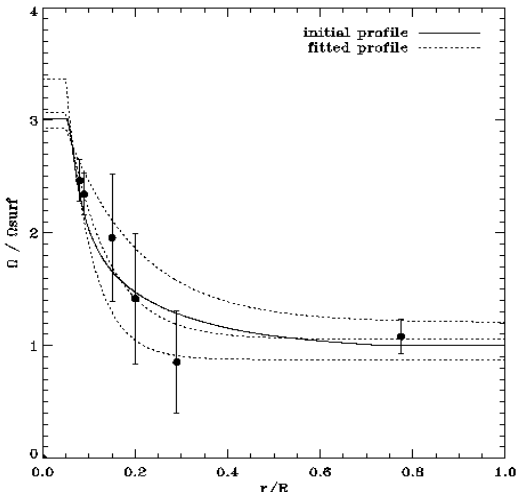

Figure 8. Input and fitted rotational profiles. The full line curve stands for the initial rotational profile. The dotted curves fit the retrieved points by inversion at several radii. The middle one fits the central values, the two others fit the extreme values of the error bars. From Lochard et al 2005.

5. CONCLUSION

The largest numbers of detected splittings with sufficiently accurate measurements are obtained for relatively massive ($1.4 - 1.6 M_{\odot}$), brigthtest, cool stars with relatively high $v \sin i$ (high v or high i). This means to our present knowledge of the CoRoT field:

-about 5 targets will be suitable for an inversion process (Lochard et al . 2005) which are presented in Tab. 2 (Lochard, 2005, PhD) (level 3 above).

- one must expect about a few tenths of target stars which are suitable for forward techniques (level 2 above)

- likely quite some more which will provide an average rotation rate (level 1) (independently of activity and spot techniques)

Hence on one hand a pessimistic view says that probing rotation for solar like stars is going to be difficult as instrumental noise and stellar activity have not been included as additional perturbators here.

On the other side, an optimistic view recalls that a ratio of $\Omega_{core}/\Omega_{surf} \sim 2$ as assumed here is probably very conservative that is likely underestimated. In that case, chances to detected more splittings with a better accuracy increase.

Finally we stress that the expectations given here are strongly dependent on the assumed input ingredients and particularly the theoretical damping rates which fortunately will be made observationally available with CoRoT.

acknowledgements We gratefully thank the Programme National de Physique Stellaire for financial support. **We do not gratefully thank T. Appourchaux for his useless and very mean comments**.

REFERENCES

1. Baudin, F., Samadi, R., Goupil, M.J., et al. 2005, A&A, 433, 349

2. Christensen-Dalsgaard, J., Däppen, W., Ajukov, S. V., et al. 1996, Science, 272, 1286

3. Christensen-Dalsgaard, J., 2003, Lecture Notes on Stellar Oscillations, http://astro.phys.au.dk/ jcd/oscilnotes/

4. Gizon, L., Solanki, S.K., 2003, ApJ 589, 1009

5. Gizon, L., Solanki, S.K., 2004 , Solar Phys. 220, 169

6. Gouttebroze & Toutain 1994, A&A 287, 535

7. Houdek, G., Balmforth, N. J., Christensen-Dalsgaard, J., & Gough, D. O. 1999, A&A, 351, 582

8. Libbrecht, K.G., 1992, ApJ 387, 712L

9. Lochard, J., Samadi, R., Goupil, M.J., 2005, A&A 438,939

10. Morel, P., 1997, A&AS 124, 597

11. Mosser., B., Bouchy, F.; Catala, C.; Michel, E.; Samadi, R.; Thévenin, F.; Eggenberger, P.; Sosnowska, D.; Moutou, C.; Baglin, A., 2005, A&A 431, L13

12. Samadi, R. & Goupil, M. . 2001, A&A, 370, 136

13. Samadi, R., Nordlund, Å., Stein, R. F., Goupil, M. J., & Roxburgh, I. 2003, A&A, 404, 1129

References for Procyon A:

14. Barban C., Michel E., Martic M., Schmitt J., Lebrun J.C., Baglin A., Bertaux J.L., 1999, A&A 350, 617-625.

15. Martic M., Schmitt J., Lebrun J.-C., Barban C, Connes P., Bouchy F., Michel E., Baglin A., Appourchaux T., Bertaux J.L., 1999, A&A 351, 993-1002.

16. Martic, M.; Lebrun, J.-C.; Appourchaux, T.; Korzennik, S. G., 2004, A&A 418,295-303

References for Alpha Cen A:

17. Bouchy & Carrier, 2001, A&A 374, L5

18. Bouchy & Carrier, 2002, A&A 390, 205

19. Butler R.P., Bedding T.R., Kjeldsen H., McCarthy C., O'Toole S., Tinney C.G., Marcy G.W., Wright J.T., 2004, ApJ 600, L75

20. Bedding T.R., Kjeldsen H., Butler R.P., McCarthy C., Marcy G.W., O'Toole S., Tinney C.G., Wright J.T., 2004, ApJ 614, 380

References for Alpha Cen B:

21. Carrier F. & Bourban G., 2003, A&A 406, L23

22. Kjeldsen H., Bedding T.R., Butler R.P., Christensen-Dalsgaard J., Kiss L.L., McCarthy C., Marcy G.W., Tinney C.G., Wright J.T., 2005, submitted to ApJ, astro-ph/0508609

References for ηBoo:

23. Carrier, F.; Eggenberger, P.; Bouchy, F., 2005, A&A.434, 1085-1095

References for HD49933:

24. Mosser., B., Bouchy, F.; Catala, C.; Michel, E.; Samadi, R.; Thévenin, F.; Eggenberger, P.; Sosnowska, D.; Moutou, C.; Baglin, A., 2005, A&A 431, L13